Supplementary Notes: Influence of timescales and data injection schemes for reservoir computing using spin-VCSELs

Lukas Mühlnickel, Jonnel A. Jaurigue, Lina C. Jaurigue,* and Kathy Lüdge†
Technische Universität Ilmenau, Institut für Physik, Weimarer Straße 25, 98693 Ilmenau, Germany
(Dated: October 25, 2024)

I. SUPPLEMENTARY NOTE 1: DYNAMICS AND PERFORMANCE WITH HIGHER BIREFRINGENCE

In the main paper the reservoir computing dynamics and performance have been investigated in the injection parameter space. The shift of the locking cone with higher birefringence was discussed and Supplementary Figure 1 now presents the full scans that were the basis for parts of the the histograms presented in the main paper. In detail, Supplementary Figure 1 shows the color coded emission dynamics of the spin-VCSEL (a), the performance with carrier (b) and phase (c) injection for a birefringence value of $\gamma_p = 30\,ns^{-1}$. The locking is shifted to lower frequency detunings due to the change in the laser frequency. Besides that an improvement in the overall performance can be seen for both injection schemes if compared to $\gamma_p = 1\,ns^{-1}$. For carrier injection the optimal regions shift to higher injection strength. The inset show zooms ino the best performing regions.

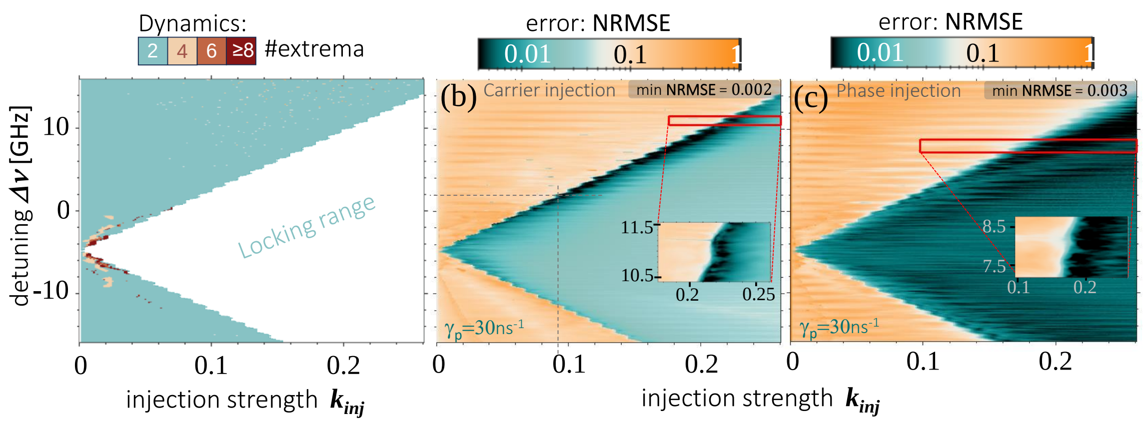

Supplementary Figure 1. Comparison of injection schemes and dynamics for high birefringence: a) Spin VCSEL dynamics found in the injection parameter space of injection strength k_{inj} and detuning $\Delta\nu$ ($k = 0.0022, \gamma_p = 30\,ns^{-1}$ (same rotating frame as for $\gamma_p = 1\,ns^{-1}$, and not corrected for the shift in laser frequency γ_p). b,c) NRMSE error with carrier and phase injection, respectively. Insets show zooms into good performing regions. Minimum error is given on the top right inset.

II. SUPPLEMENTARY NOTE 2: DIFFERENT TASKS, SPIN RELAXATION TIME AND MODULATION RESPONSE

Throughout the paper we used a one step ahead prediction task for the x-coordinate, i.e. the output of the laser intensity is used to predict one discrete time step into the future after a sampling time step of $\Delta_d = 0.1$ of the Lorenz x-coordinate was used. In Supplementary Figure 2b we show its prediction performance as a function of the spin relaxation time for carrier injection into m (orange curve) but we also show the more complicated cross-prediction task were the z-coordinate is to be predicted after injecting the x-coordinate (green line). Here a smaller sampling time step of $\Delta_d = 0.02$ is used. Overall a similar dependence on the spin relaxation rate is found. For the phase injection scheme, instead, the spin relaxation does not change the performance as can be seen by the green line in Supplementary Figure 2a.

* Email address: lina.jaurigue@tu-ilmenau.de
† Email address: kathy.luedge@tu-ilmenau.de

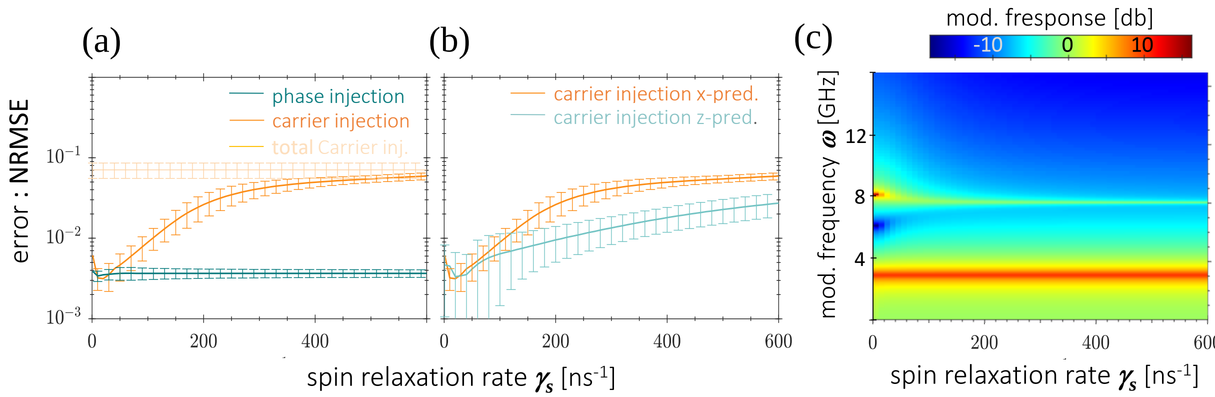

Supplementary Figure 2. Impact of spin relaxation rate: Computing error as a function of γ_s for a) carrier-, phase and total carrier injection (orange, green and light orange curve), b) two different prediction task (orange: x-prediction (stepsize $\Delta_d = 0.1$) and green: z-prediction (stepsize $\Delta_d = 0.02$), c) modulation response of the solitary spin-VCSEL after modulating the pump polarization (color code indicates the normalized modulation response in db). Parameters: $\gamma_p = 30\, ns^{-1}$, $k = 0.0022$.

In Supplementary Figure 2c we depict the modulation response of the solitary spin-VCSEL color coded as a function of the spin relaxation rate γ_s. We can see that the additional resonance at a modulation frequency of 8 GHz decreases with γ_s and for values $\gamma_s > 400\, ns^{-1}$ only the peak resulting from the relaxation oscillation at $3GHz$ remains.The fast beating oscillation are exploited for the case of carrier injection but they are not addressed for phase injection.

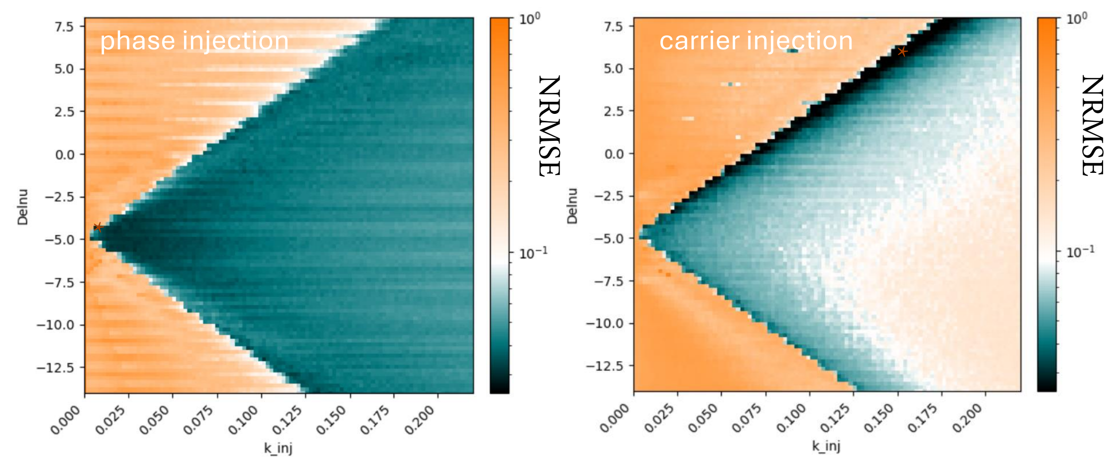

Supplementary Figure 3. Lorenz cross prediction: One step ahead prediction performance (sampling step $\Delta_d = 0.1$) plotted color coded in the injection parameter space $(\Delta\nu, k_{inj})$. Left panel shows phase injection (best performance is 0.029 ± 0.0022) while right panel shows carrier injection into the charge carrier difference m (best performance is 0.01 ± 0.002). Parameters: $T = 1ns$, $\tau = 1.41ns$, $\gamma_s = 10ns^{-1}$,$\gamma_p = 30ns^{-1}$, $k = 0.0022$.

We also implemented the Lorenz cross prediction for a one step ahead prediction with a sampling step of $\Delta_d = 0.1$. The results are plotted in Supplementary Figure 3. The same trends regarding the good performance regions can be observed. The overall performance is worse as the task is more difficult for the reservoir to learn.

III. SUPPLEMENTARY NOTE 3: DYNAMICS UNDER VARYING FEEDBACK PHASE AND FEEDBACK STRENGTH

In this section we want to discuss in more detail the changes in the bifurcation scenario with increasing injection strength. Supplementary Figure 4 shows numerical results of the dynamic behaviour found for a laser with optical injection and feedback. Different to the spin-VCSEl discussed in the other part of the paper and supplementary, we used a quantum-dot (QD) laser for the simulations. The QD laser has more strongly damped and less pronounced relaxation oscillations which makes it less vulnerable to optical feedback and makes the characterization easier. Besides that the trends are analogous as they are an effect of the field interactions with the delayed version of the field, which are similar for different types of lasers and mainly depend on the damping of the relaxation oscillations [1]. Note that feedback and injection strength are scaled differently by a factor of 2 than in the spin-VCSEL model used in the main paper (spin VCSEL values are smaller). All parameters for the QD laser can be found in [2].

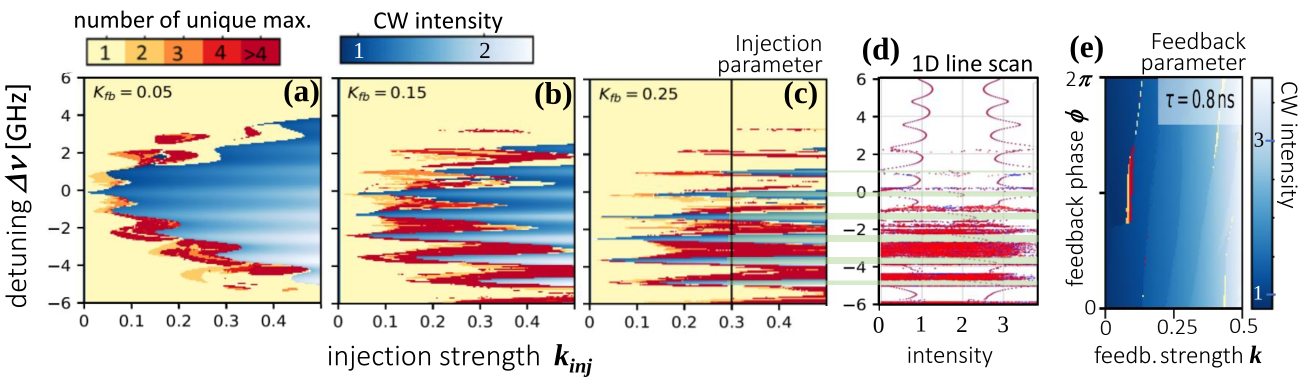

Supplementary Figure 4. Bifurcation structure of a laser with optical injection and feedback: (a)-(c) Quantum dot laser dynamics with optical injection and self-feedback with $\tau = 0.8ns$ in the injection parameter space $(\Delta\nu, k_{inj})$. The dynamics is color coded in all panels with blue giving the normalized cw intensity and yellow/red colors encoding the number of unique maxima. (d) One parameter bifurcation scan along increasing detuning $\Delta\nu$ (indicated by the vertical line in (c)) with the intensity of the extrema plotted as red points .(e) 2-dim. scan of the dynamics in the feedback parameter plane (without optical injection) showing the effect of the feedback phase ϕ and strength k (color code is the same as in (a-c)).

The evolution of the unlocking transitions (border of the blue region) with increasing feedback strength can be seen by comparing Supplementary Figure 4(a),(b) and (c). Stronger feedback (Supplementary Figure 4c) leads to a complete separation of the stable regions with cw operation (blue colors) with most of the parameter plane being filled with signatures of chaotic dynamics (red colors). In the regions with only one maximum (yellow colors in (a-c)) a simple oscillation is found. Panel (d) shows a line scan along increasing detuning (y-axis) with the intensity of the observed extrema plotted in red (x-axis). The effect of the feedback phase is visualized by scanning the dynamics as a function of feedback strength and feedback phase. The different blue shading originate from stable emission at different external cavity modes.

IV. SUPPLEMENTARY NOTE 4: IMPACT OF VIRTUAL NODE DISTANCE ON PERFORMANCE

In the main text we state that an optimal virtual node distance is given by a value of $\theta = 33\,ps$. Supplementary Figure 5 shows the performance as a function of the clock cycle T and the delay time τ. virtual node distance θ (the median value after averaging over 10 different masks is plotted). The number of virtual nodes N_v is not changed in order to not mix the results with the effect of an increasing readout dimension [3, 4]. This means that changing T effectively changes the virtual node distance θ. In the Supplementary Figure it can be seen that the ratio between clock cycle and delay time dramatically change the performance as was also discussed elsewhere [3, 5]. The dark regions of good performance are centered around a ratio of $\tau/T \approx \sqrt{2}$ which has been proven before to be a good choice [3, 5]. For the phase injection that is plotted in Supplementary Figure 5a, a faster readout is possible (see red star) while for carrier injection longer clock cycle values and thus longer θ are better. Comparing the minimum performance values possible the phase injection is much better at this very high injection strength of $k_{inj} = 0.22$ for smaller injection strength of $k_{inj} = 0.059$ as also discussed in the main paper, the carrier injection leads to the overall best results (Supplementary Figure 6).

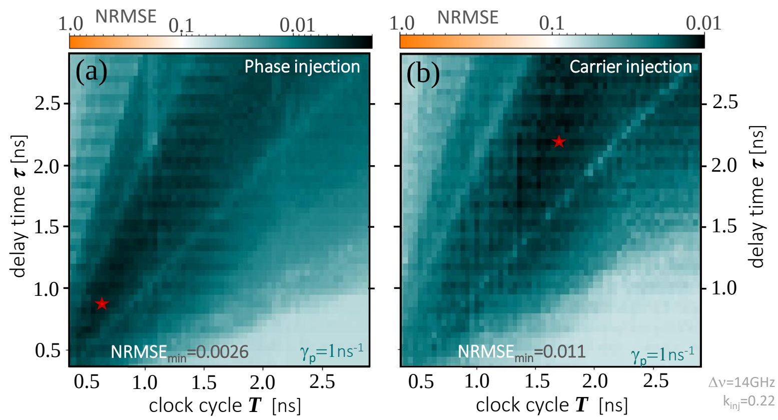

Supplementary Figure 5. Prediction performance NRMSE error as a function of the delay time τ and the clock cycle $T = 30 \times \theta$. NRMSE error is color coded as given by the color bar. Red stars mark positions with optimal performance. (a) phase injection scheme (b) carrier injection scheme for $\gamma_P = 1\,ns^{-1}, \Delta\nu = 14GHz, k_{inj} = 0.22$

.

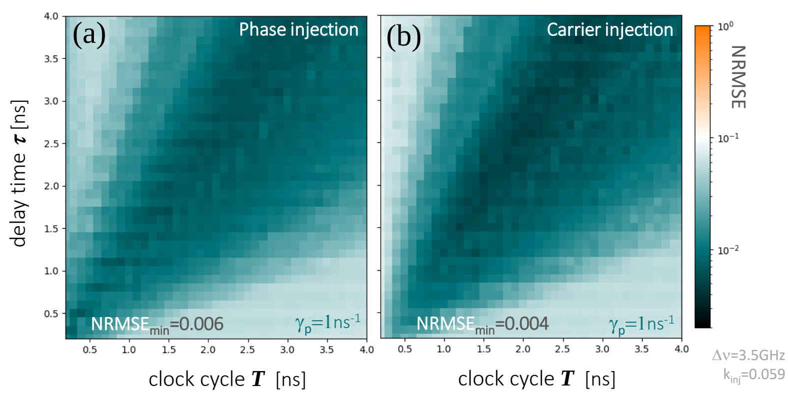

Supplementary Figure 6. Prediction performance NRMSE error as a function of the delay time τ and the clock cycle $T = 30 \times \theta$. (a) phase injection scheme (b) carrier injection scheme for $\gamma_P = 1\,ns^{-1}, \Delta\nu = 3.5GHz, k_{inj} = 0.059$

V. SUPPLEMENTARY REFERENCES

[1] K. Lüdge and B. Lingnau, Laser dynamics and delayed feedback, isbn 978-1-07-160420-5 (Springer Nature, New York, NY 10004, 2020) pp. Synergetic–18, 1st ed.

[2] F. Köster, B. Lingnau, A. Krimlowski, P. Hövel, and K. Lüdge, Collective coherence resonance in networks of optical neurons, Phys. Status Solidi B **2021**, 2100345 (2021).

[3] A. Röhm, L. C. Jaurigue, and K. Lüdge, Reservoir computing using laser networks, IEEE J. Sel. Top. Quantum Electron. **26**, 7700108 (2019).

[4] F. Köster, S. Yanchuk, and K. Lüdge, Insight into delay based reservoir computing via eigenvalue analysis, J. Phys. Photonics **3**, 024011 (2021).

[5] T. Hülser, F. Köster, L. C. Jaurigue, and K. Lüdge, Role of delay-times in delay-based photonic reservoir computing, Opt. Mater. Express **12**, 1214 (2022).